Int J Adv Manuf Technol (2015) 76:1225–1242
DOI 10.1007/s00170-014-6355-9

ORIGINAL ARTICLE

Dynamic characteristics optimization for a whole vertical machining center based on the configuration of joint stiffness

Congying Deng · Guofu Yin · Hui Fang · Zhaoyuxi Meng

Received: 24 March 2014 / Accepted: 5 September 2014 / Published online: 16 September 2014

Abstract Joint stiffness often has a significant effect on the dynamic characteristics of the whole machine tool. In this paper, a joint stiffness configuration method is developed to optimize the dynamic characteristics of a whole vertical machining center, in which the premise is considering the joint characteristics to create the accurate finite element model (FEM) of the whole machine tool. Identifying the joints parameters including the contact stiffness and damping of the linear guides, bolts, ball screws, and bearings is conducted. Vibration test and finite element simulation are implemented to verify the accuracy of the FEM which is created based on the identified joints parameters by comparing the tested and simulated frequency-response functions (FRFs). With these tested and simulated results, taking the dynamic flexibility at the spindle nose to measure the dynamic characteristics of the whole machine tool, vibration modes, and joints related to a higher modal flexibility and elastic energy distribution ratio can be determined to be the weak modes and joints respectively. Optimization aiming to decrease the modal flexibility is conducted by adopting the orthogonal experiment method to instruct the simulations to predict how stiffness of the weak joints affected the dynamic characteristics of the whole vertical machining center. Thus, an optimal joint stiffness configuration can be obtained by using the range analysis and fuzzy similar preference ratio method to analyze the simulated results. Redoing the simulation with the optimal configuration, results indicate that modal flexibility of each weak mode is decreased obviously. The decreased modal flexibilities and dynamic responses verify that the optimal configuration method is feasible to provide a way for improving the dynamic characteristics of the whole machine tool.

C. Deng (✉) · G. Yin · H. Fang · Z. Meng
School of Manufacture Science and Engineering,
Sichuan University, Chengdu 610065, China
e-mail: 413880059@qq.com

Keywords Joint stiffness · Whole vertical machining center · Modal flexibility · Orthogonal experiment · Energy distribution

1 Introduction

Machine tool dynamic behaviors refer to its ability to resist the vibrations in the machining process, including the vibration resistance and stability. The machine tool is composed of many components in a particular way, such as the bolt connection, the guide-slide connection, the welding, etc. The existence of various joints destroys the continuity of a machine tool, which cause its dynamic behaviors are not only affected by the components, but also by the dynamic characteristics of these joints [1, 2]. Researches show that about 60 % of the total dynamic stiffness and about 90 % of the total damping are caused by the joints [3]. It is significant to study how the joint dynamic characteristics affect the dynamic behaviors of a whole machine tool. Researches about the joints are mainly focused on the dynamic modeling of the joint, joint characteristics identification and the dynamic behaviors of a whole machine tool based on joints [4–14].

Ahmadian et al. [15] proposed a nonlinear model for bolted lap joints and interfaces, in which the joint interface was modeled by using a combination of linear and nonlinear springs and a damper to simulate the dynamic characteristics of the joints. Parameters of the springs and damper were identified by minimizing the difference between the model predictions and the experimental data. Mao et al. [16], according to the inverse relationship between the frequency-response function matrix and the dynamic stiffness matrix of a Multidegree-of-Freedom system, proposed a high-accuracy parameter identification method which recognized the dynamic parameters of the fixed joints based on the dynamic experiment data of the whole structure including the joints. The

effectiveness and accuracy of the identification method had been validated. Lin et al. [17], on the basis of the finite element simulation and vibration experiment found that the linear guide-slide joint was the key factor that affects the dynamic characteristics of the spindle-column system. With the increasing preload of the linear guide joint, the dynamic characteristics of the spindle-column system could be improved. Wu et al. [18] introduced the Hertzian contact theory and applied normal/shear stiffness to contact elements in the overall finite element model to study the dynamic characteristics of the linear guides affected by preload. Yoshihara [19] established a lumped mass beam dynamic model of a two-pillar vertical lathe, in which there were 20 joint surfaces with two rail joints and the rest bolted joints. The experiment results verified this model which took the characteristics of joints into account to be accurate. Park et al. [20] proposed an enhanced receptance coupling methodology by identifying the joint dynamics between substructures through experimental and finite element (FE) analyses. With the identified parameters, dynamic properties of the modular tools could be predicted, enabling designers to optimize dynamic behavior in the conceptual stage.

As various types of joints exist in a machine tool and each joint has different dynamic parameters under different contact conditions, it is difficult to study the influences to the dynamic behaviors of a machine tool from each joint. Researches which consider the synthetical influences of each joint to the dynamic behaviors of a machine tool and provide an effective way to optimize the dynamic characteristics are relatively few [21, 22].

The purpose of this paper is to propose an optimal configuration method of the joints stiffness for improving the dynamic characteristics of a whole vertical machining center. To create an accurate FEM of the vertical machining center, in which the contact parameters of the linear guide, bolt joint, ball screw, and bearing are taken into consideration, approaches to identify the contact stiffness and damping are developed. The accuracy of the FEM is verified by comparing the measured and simulated FRFs at the spindle nose. Utilizing the dynamic flexibility to measure the dynamic behaviors of the vertical machining center, modal flexibility and elastic energy distribution theory are adopted to determine the weak modes and joints respectively. A multiobjective optimization model aiming to improve the dynamic behaviors of the vertical machining center is constructed in which the contact stiffness of each weak joint and the minimal modal flexibility of each weak modes are regarded as the design variables and the objectives respectively. Using the orthogonal experiment method to instruct the simulations of the optimization, the optimal configuration of the joints is obtained by adopting the range analysis and fuzzy similar preference ratio method to analyze the simulated results. Redoing a simulation with the optimal configuration, the decreased modal flexibility and dynamic responses validate the feasibility of this optimization method.

2 Vertical machining center and its joints

The whole vertical machining center studied in this paper is mainly composed of the spindle, the headstock, the column, the bed, the saddle, and the worktable as shown in Fig. 1. The automatic tool changing system and the electrical cabinet are simplified as the equivalent blocks. The vertical machining center has three axes, and its worktable, saddle, and headstock travels in the *X*, *Y*, and *Z* direction respectively. According to researches, there are four types of joints in the vertical machining center. These joints are linear guide, bolt joint, bearing, and ball screw [23, 24].

To establish the accurate FEM of the whole vertical machining center, in which the joints stiffness and damping are taken into consideration, we have aimed to identify these contact parameters and create their dynamic models.

3 Joints simplification and identification

In this section, dynamic modeling and contact parameters identification of the joints are discussed.

3.1 Stiffness and damping identification of linear guide

The dynamic stiffness and damping of the linear guide are identified based on the modal frequency and damping ratio. The identification process combines the finite element analysis and the modal experiment.

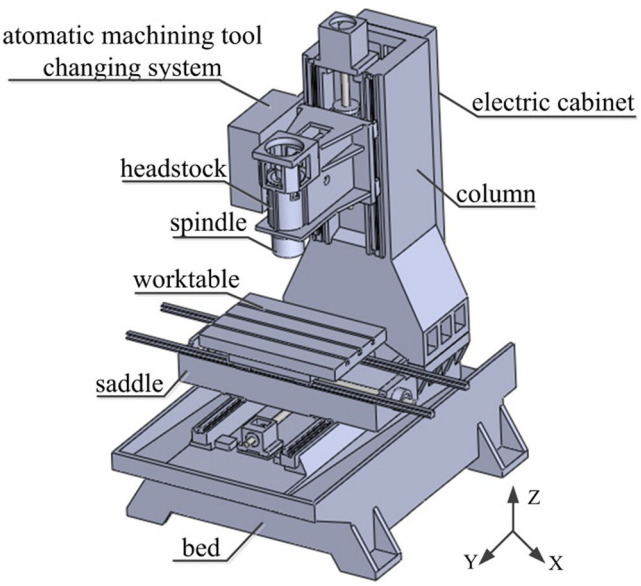

Fig. 1 The studied vertical machining center

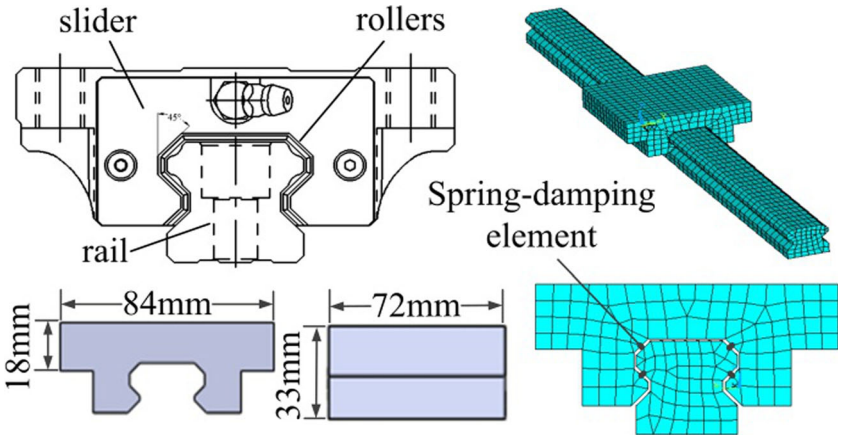

Fig. 2 Dynamic model of the linear guide

The linear guide is composed of a rail, a slider, and several rollers as shown in Fig. 2.

The rail and the slider are mainly made of alloy steel, whose elastic modulus E is 206 GPa, density ρ is 7800 kg/m^3, and Poisson's ratio μ is 0.3. The mass of the slider is 1.09 kg, and its geometric dimensions are also shown in Fig. 2. In the FEM of the linear guide, the rail and the slider were meshed with brick elements. Ignoring the mass of the rollers, we used eight spring-damping elements to connect the slider and the guides described in Fig. 2.

With the estimated dynamic stiffness and damping coefficients in the FEM, a modal analysis can be simulated in the finite element analysis software. Thus, ranges of natural frequencies, damping ratios, and vibration modes can be obtained.

A modal experiment of the linear guide was carried out to get the natural frequencies, damping ratios and vibration modes. The typical vibration modes of a linear guide are characterized as pitching, rolling, yawing, and vertical motions as shown in Fig. 3.

To measure the vibration motions of the linear guide, an accelerometer was adopted to obtain the vibration responses in different directions. As the studied linear guide system belonging to a small size structure, choosing an impulse hammer to perform the single-point excitation could input enough energy to the system to have the satisfied FRFs. In the experiment, the linear guide was fixed and positions to mount the accelerometer were determined by the points that had the largest amplitudes in any one of the three directions, which had been predicted by the finite element modal analysis. Only one accelerometer was chosen to pick up the outputs avoiding causing too much added mass to the slider; thus, we divided the vibration experiment into three parts for measuring the signals at the positions A, B, and C, respectively, as shown in Fig. 4. Position A was used to measure the vertical motion of the slider, position B was for the rolling and pitching vibrations and position C was for the yawing vibration [10, 18].

We adopted the vibration testing system of LMS Company to collect and process the data to get the FRFs. With the FRFs, the natural frequencies, the damping ratios and the vibration modes of the linear guide were obtained by its modal analysis module. The impulse hammer was with a force sensor and a steel tip. Thirty-nine different points were determined as the positions to exert the exciting force as shown in Fig. 4. To get the direct FRFs at the points mounted by accelerometer, the hammer had been as close as possible to the accelerometer when excited at the positions A, B, and C. Parameters related to the impulse hammer and accelerometer are illustrated in Table 1.

The stiffness and damping of the linear guide are identified based on the optimal algorithm. If the natural frequency and damping ratio errors between the modal experiment and

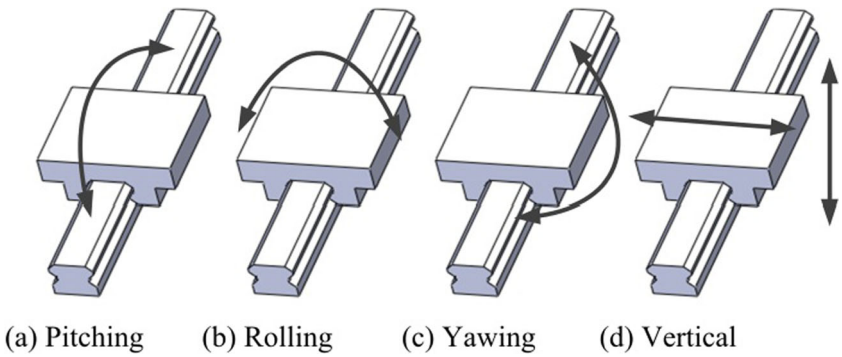

Fig. 3 Typical vibration modes of a linear guide

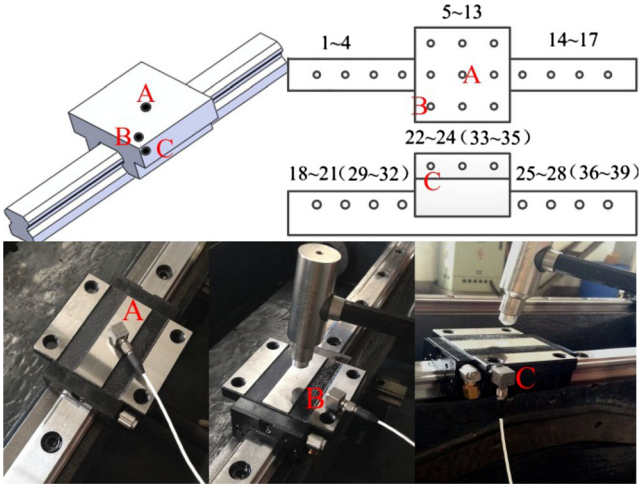

Fig. 4 Modal experiment of the linear guide

simulation are acceptable, the stiffness and damping coefficients estimated in the simulation can be regarded as the dynamic stiffness and damping coefficients of the linear guide. The process of the identification is as follows:

1. Taking the natural frequencies and damping ratios of the experiment and the simulation to establish the objective functions, the stiffness coefficient k and the damping coefficient c are regarded as the designed variables. The objective functions are given as follows:

$$\min f(k) = \sum_{i=1}^{n} \left(\frac{\omega_i^c - \omega_i^e}{\omega_i^e} \right)^2 \leq \varepsilon_1 \tag{1}$$

$$\min f(c) = \sum_{i=1}^{n} \left(\frac{\xi_i^c - \xi_i^e}{\xi_i^e} \right)^2 \leq \varepsilon_2 \tag{2}$$

where ω_i^c and ξ_i^c are the ith natural frequency and damping ratio calculated by the simulation, ω_i^e and ξ_i^e are the ith natural frequency and damping ratio obtained from the modal experiment, i is the mode order, n is the number of fitted modes, ε_1 is the acceptable stiffness error, and ε_2 is the acceptable damping ratio error.

2. Using a program to realize the interaction of the numerical calculation software and the finite element analysis software automatically. The numerical calculation software transfers the initial stiffness and damping coefficients to the finite element analysis software to actuate the modal analysis. After the analysis, the modal information is transferred to the numerical calculation software to calculate and compare the errors. Repeat this process until the errors are in the acceptable range.

The stiffness and damping coefficients identified by this optimal algorithm are 6.07×10^8 N/m and 5280 N s/m.

Tables 2 and 3 show the experimental results, simulated results, and their errors. The natural frequency and damping ratio errors show that the established FEM of the linear guide can be used to describe the dynamic characteristics of the linear guide [10, 18].

Table 1 Parameters related to the vibration experiment

Name	Type	Sensibility	Weight
Accelerometer	ICP	99.8 mV/g	4.0 g
Impulse hammer	PCB 086D05	0.23 mV/N	0.32 kg

Table 2 Natural frequency comparison between experiment and simulation

Order	Experiment (Hz)	Simulation (Hz)	Error (%)	Vibration mode
1	986.7	985.6	0.1	Rolling
2	3022.1	3025.9	0.03	Vertical ↕
3	3427.6	3592.2	4.80	Vertical ↔
4	3567.8	3647.6	2.23	Yawing

3.2 Stiffness and damping identification of bolt joint

As one typical kind of fixed joint, the bolt joint distributes widely in the vertical machining center. Its dynamic characteristics are affected by the pressure, geometry shape, materials, surface roughness, etc. [4, 20, 25].

One typical bolt joint which includes part A, Part B, a bolt and a nut in the vertical machining is shown in Fig. 5b. Figure 5a shows the torque condition of the nut, in which T is the tightening torque, T_a is the friction moment from the screw pair, and T_b is the friction moment due to the interface between the nut and part B. According to the moment equilibrium condition of the nut, we can get Eq. (3).

$$T = T_a + T_b \tag{3}$$

T_a and T_b are calculated by Eq. (4) to Eq. (6).

$$T_a = \frac{D_0}{2} F_t \tag{4}$$

Table 3 Damping ratio comparison between experiment and simulation

Order	Experiment (%)	Simulation (%)	Error (%)
1	1.54	1.57	1.57
2	1.43	1.46	1.46
3	1.81	1.83	1.83
4	1.65	1.64	1.64

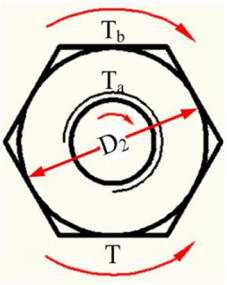

(a) The torque condition of the nut

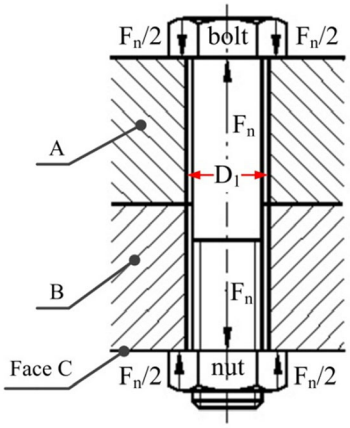

(b) The force condition of the bolt and the components

Fig. 5 The blot joint and its loading conditions

$$T_b = f_c r_n = \mu_c F_n r_n \tag{5}$$

$$r_n = \frac{\left(D_2{}^3 - D_1{}^3\right)}{3\left(D_2{}^2 - D_1{}^2\right)} \tag{6}$$

Where F_t is the circumferential force of the thread pair, D_0 is the nominal diameter of the nut, f_c is the friction force between the nut and face c (Fig. 5(b)), F_n is the axial force between the nut and face c, μ_c is the friction coefficient between the nut and the face c, r_n is the equivalent frictional radius of the nut, and D_1 and D_2 are marked in Fig. 5.

In one screw pair, the axial load of the nut is distributed along the thread. To simply the analysis, take a concentrated load to replace the axial load and assume that it acts on one point which locates at the circumference of a circle with the pitch diameter. The load condition of a nut can be divided into two situations based on the thread angle.

1. The thread angle is zero

   When the thread angle is zero, the profile of the thread is a rectangle as shown in Fig. 7b. Spreading the thread along the circumference of a circle with the pitch diameter, one slope can be obtained as shown in Fig. 6.

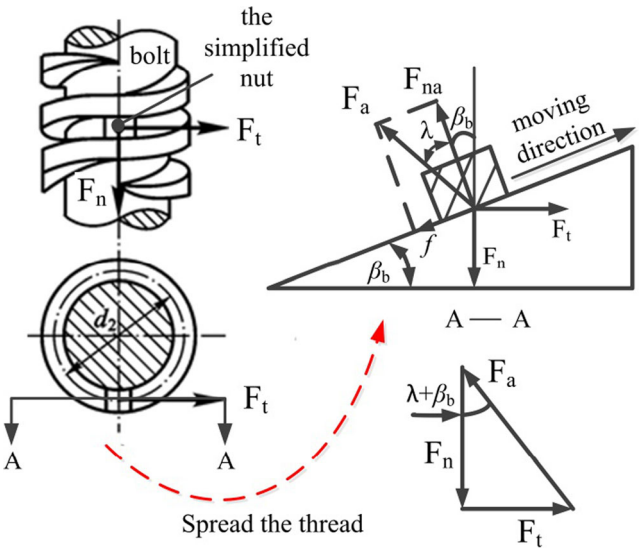

Fig. 6 Force condition of a nut with rectangular thread profile

The slope angle is equal to the lead angle. When the nut rotates and has a rise in the axial direction, the nut is regarded as a slider which moves up along the slope. The force condition is shown in Fig. 6, in which F_t is the circumferential force of the thread pair, F_n is the axial force and β_b is the lead angle. According to the force condition of the nut, we can get Eq. (7) and Eq. (8).

$$F_t = F_n \tan(\lambda + \beta_b) \tag{7}$$

$$\arctan\lambda = \frac{\mu_1 F_{na}}{F_{na}} = \mu_1 \tag{8}$$

Where μ_1 is the friction coefficient between the bolt and the nut.

With Eq. (3) to Eq. (7), F_n can be calculated.

$$F_n = \frac{2T}{D_0 \tan(\lambda + \beta_b) + 2\mu_c r_n} \tag{9}$$

2. The thread angle is not zero

   When the thread angle is 2α, profile of the thread is like a triangle shown in Fig. 7a. The nut is regarded as a wedge, which moves up on another wedge that locates at one slope with a slope angle equaling to the lead angle. The force condition of the nut is shown in Fig. 8. From Fig. 8b, we can see that the existence of the thread angle affects the normal force of the interface between the nut and the bolt.

   According to the force condition of the nut, we can get Eqs. (10) and (11).

$$F_t^w = F_n^w \tan(\lambda^w + \beta_b) \tag{10}$$

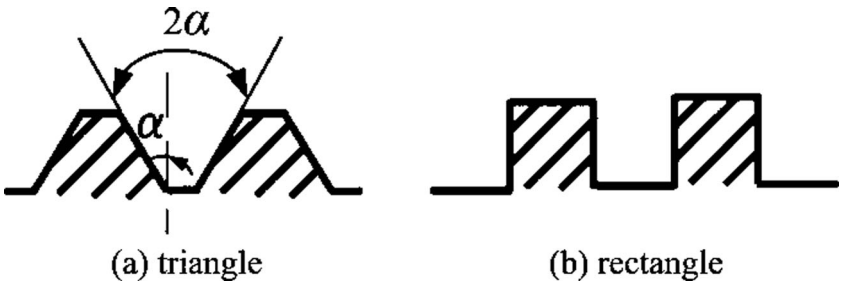

Fig. 7 Profiles of the thread

$$\arctan\lambda^w = \frac{\mu_1 F_{na}^{wn}}{F_{na}^{wn}\cos\alpha} = \frac{\mu_1}{\cos\alpha} \tag{11}$$

Then, F_n^w can be calculated by Eq. (12).

$$F_n^w = \frac{2T}{D_0\tan(\lambda^w + \beta_b) + 2\mu_c r_n} \tag{12}$$

Based on Eqs. (6), (8), (9), (11), and (12), F_n can be obtained by Eq. (13).

$$F_n = \frac{2T}{D_0\tan(\rho_v + \beta_b) + 2\mu_c \frac{\left(D_2{}^3 - D_1{}^3\right)}{3\left(D_2{}^2 - D_1{}^2\right)}} \qquad \rho_v = \arctan\mu_1/\cos\alpha \tag{13}$$

Where ρ_v is the equivalent friction angle. When it equals zero, it meets the first condition. When it does not equal zero, it meets the second condition.

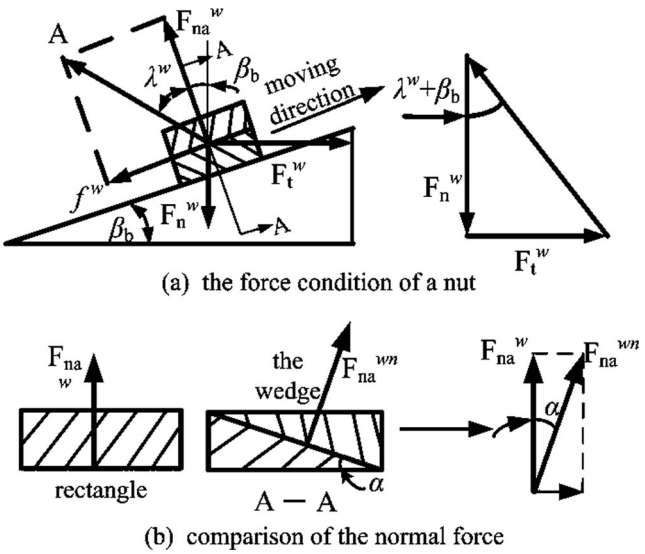

Fig. 8 Force condition of a nut with triangular thread profile

The pressure of the bolt joint is described as Eq. (14).

$$P_n = \frac{2T}{\left[D_0\tan(\rho_v + \beta_b) + 2\mu_c \frac{\left(D_2{}^3 - D_1{}^3\right)}{3\left(D_2{}^2 - D_1{}^2\right)}\right]A} \tag{14}$$

Where A is the area of bolt joint.

In many situations, the bolt joint has many bolts. Supposing the force of each bolt is equal, which is accurate enough in engineering [23], the pressure of bolt joint is calculated by Eq. (15):

$$P_n = \frac{2T}{\left[D_1\tan(\rho_v + \beta_b) + 2\mu_c \frac{\left(D_2{}^3 - D_1{}^3\right)}{3\left(D_2{}^2 - D_1{}^2\right)}\right]AN} \tag{15}$$

Where N is the number of bolts.

Researches have widely discussed how the pressure affects the dynamic characteristics of the bolt joint [26–29]. Researches have presented the contact stiffness and damping under different pressure. With the pressure calculated by Eq. (15), we can obtain the contact stiffness and damping under the same contact conditions by consulting these researches. In this paper, the contact stiffness and damping of the bolt joint are obtained from Refs. [28] and [29].

3.3 Dynamic modeling of bearing and ball screw

1. Bearing

   Avoiding the complexity to create and mesh the 3D model of the bearing, the balls and ball groove are ignored. The inner ring and outer ring were connected by elastic spring elements as shown in Fig. 9. The contact stiffness was obtained from the product selection guide [13].
2. Ball screw

   As a transfer component with high precision and efficiency, the ball screw studied in this paper is used in the

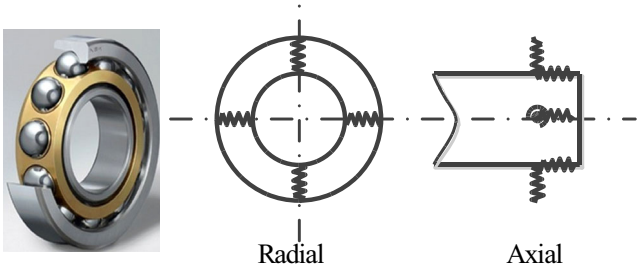

Fig. 9 The bearing

feeding device of a machine tool to carry the major load in the feeding direction. The studied ball screw and its simplified 3D models are shown in Fig. 10. To draw the 3D models conveniently, the helical groove around the screw shaft and the nut are ignored. The axial and radial stiffness of the ball screw is determined based on the properties of the screw and nut and their geometrical relationship. The contact stiffness can be obtained from the manufacturer [17, 18, 30].

4 FEM of the vertical machining center

The process for establishing the FEM of the vertical machining center is mainly discussed as follows:

1. Simplification of the components
   To save the meshing time, components with complex structures were simplified according to some certain principles. All the structures were meshed by solid elements.
2. Simulation of the joint interfaces

   Linear guide. The simulation of linear guide interface is shown in Fig. 2.

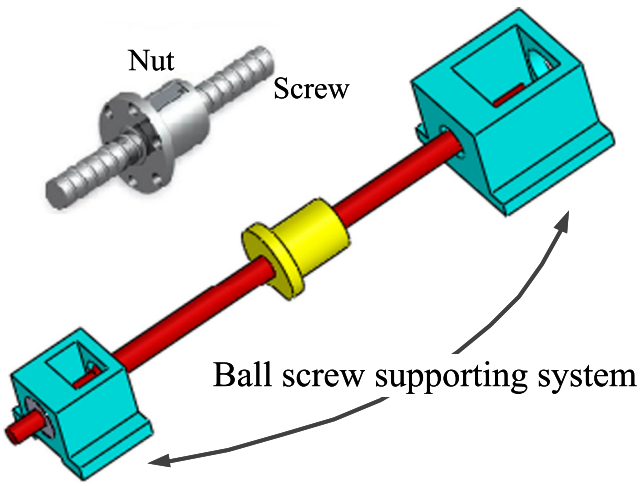

Fig. 10 The studied ball screw

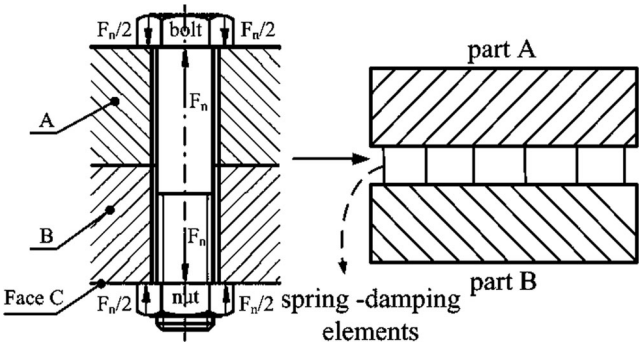

Fig. 11 Simulation of bolt joint

Bolt joint. The simulation of bolt joint interface is shown in Fig. 11. Table 4 lists the identified contact parameters of column-bed bolt joint.

Bearing. The FEM of the bearing was created based on Figs. 9 and 12a, in which the mass of the outer ring, the balls and the inner ring were ignored. Stiffness matrix elements are distributed evenly around the shaft to simulate the axial and radial stiffness as shown in Fig. 12a. Overall contact stiffness of each bearing obtained from the manufacturer is listed in Table 5.

Ball screw. The specifications of the ball screw are listed in Table 6. The screw shaft and the nut were meshed by solid elements as shown in Fig. 12c. The contact stiffness at the screw groove were obtained according to the technical guides, which is 264, 248, and 149 N/μm in the *X*, *Y*, and *Z* directions respectively [31]. To simplify the modeling process, the shaft and nut were bonded together, and the spring elements between the load and nut were used to simulate the axial contact stiffness between the nut and screw.

Considering the characteristics of these joints, FEM of the whole vertical machining center was established as shown in Fig. 13. Joints characteristics were simulated by the spring-damping elements and the stiffness matrix elements.

5 Finite element analysis of the whole machining center

With the FEM of the whole vertical machining center, the modal analysis and harmonic analysis can be simulated.

The modal analysis is simulated to predict the inherent properties of the vertical machining center, including the natural frequencies and mode shapes. According to the frequencies, the vertical machining center can avoid working near them in the machining process. The mode shapes represent the vibrations of the whole vertical machining center,

Table 4 The identified contact parameters of column-bed joint

Joint	Material	Rough degree	Pressure (MPa)	Normal		Tangential	
				Stiffness (N/m)	Damping (N·s/m)	Stiffness (N/m)	Damping (N·s/m)
Column-bed	Cast iron-cast iron	1.6	5.04	4.63×10^{10}	1.08×10^{6}	6.9×10^{9}	1.12×10^{5}

which relate to the excitations and the relative displacement between different components, revealing its weak parts. Focusing on the frequencies below 600 Hz, the fundamental vibrations of the studied vertical machining center are depicted in Fig. 14.

As described in Fig. 14a, the column and the headstock have a bending vibration in the *YZ* plane at the first natural frequency 52.1 Hz. The column and the headstock have a sway movement in the *XZ* plane at frequency 77.3 Hz as shown in Fig. 14b. The headstock has a rotation around the *Z* axis at the frequency 155.7 Hz as shown in Fig. 14c. The headstock has a bending vibration in the *YZ* plane at the frequency 165.2 Hz as shown in Fig. 14d. Figure 14e shows the rotation of the worktable and the saddle around the *Z* axis. Figure 14f shows the micro vibration of the bed.

Harmonic analysis is simulated to predict the frequency response of the whole vertical machining center caused by the external excitation. The amplitude of the external excitation is 1 N, and the directions are illustrated in Fig. 15. Three simulations were conducted to obtain the direct frequency responses of accelerance at the spindle nose in *X*, *Y*, and *Z* directions respectively, and the results are described in Fig. 16.

The maximum accelerance of the FRF in the *X*, *Y*, and *Z* direction is 0.383 $m/s^2/N$ at frequency 509.2 Hz, 0.144 $m/s^2/N$ at frequency 540.6 Hz and 0.716 $m/s^2/N$ at frequency 551.8 Hz, respectively. In the frequency range 0~600 Hz, the whole machining vertical center has a poor vibration resistance in *X* and *Z* direction. Comparing these FRFs, we can find some connections between two FRFs. For example, there is a peak of the FRF in *X* and *Z* direction respectively at the frequency 217.9 Hz, which is caused by the torsion of the headstock in the *XZ* plane.

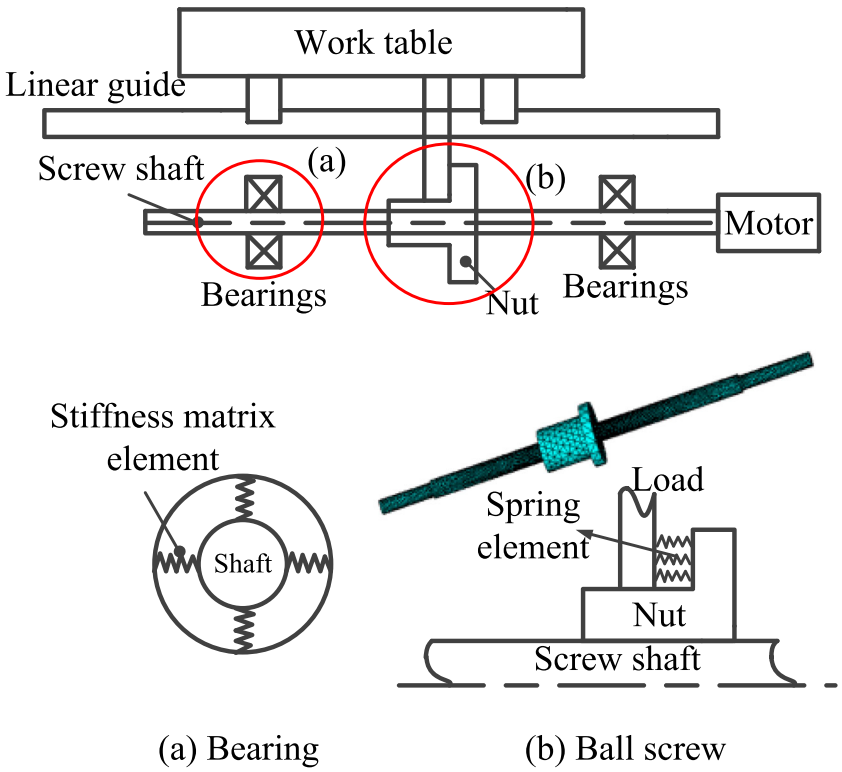

Fig. 12 Interface simulations of the bearing and the ball screw

Table 5 Basic parameters of the bearings

	Outer diameter D/mm	Inner diameter d/mm	Width B/mm	Contact angle β	Preload P/N	Stiffness of bearing	
						Axial (/N/m)	Radial (/N/m)
7012C	60	95	18	15	100	5.3×10^{7}	3.45×10^{8}
25TAC62B	62	25	15	60	1490	7.33×10^{8}	–

Table 6 Basic parameters of the ball screw

Nominal diameter d_o/mm	Ball diameter d_b/mm	Travel P_t/mm	Contact angle β/(°)	Rows×turns	Rigidity (N/μm)
32	6.35	16	45	1×3.5	672

6 Vibration experiment of the whole vertical machining center

The vibration experiment was conducted to measure the characteristics of the whole vertical machining center and verify the accuracy of the FEM. The experimental devices included the impact hammer, the acceleration sensors, the LMS vibration testing system, and a personal computer as shown in Fig. 17.

In the experiment, the external exciting force was exerted by the impact hammer and we moved the hammer to exert the exciting force at different parts of the whole vertical machining center. The hammering positions were arranged to avoid at the nodal points predicted by the finite element modal analysis. Three acceleration sensors were pasted at the spindle nose marked as X, Y, and Z to obtain the response signals in three directions as shown in Fig. 18. Parameters related to the impact hammer and acceleration sensors are listed in Table 7. The force and accelerance signals were recorded by the LMS vibration testing system, which were processed to obtain the FRFs. When hammering at the positions marked as X, Y, and Z to get the direct FRFs, the hammer was as close as possible to these acceleration sensors. Taking the working conditions of the machine tool into consideration, we focused on the dynamic characteristics between 0 and 600 Hz.

The measured direct frequency responses of accelerance at the spindle nose in X, Y, and Z directions are depicted in Fig. 19. Comparing the measured FRFs in Fig. 19 with the simulated FRFs in Fig. 16, the measured curves agree well with the simulated curves in the same directions. Frequencies corresponding to the peaks are also in good agreement in the same directions. Table 8 lists the experimental and simulated natural frequencies and their relative errors. All these errors are close or below 10 %, which meet the requirement of the project cooperated by our team and the machine tool producer. Thus, we regarded that the FEM of the whole machining center was established accurately and the FEM could be used in predicting the characteristics of the whole vertical machining center [3, 23, 32].

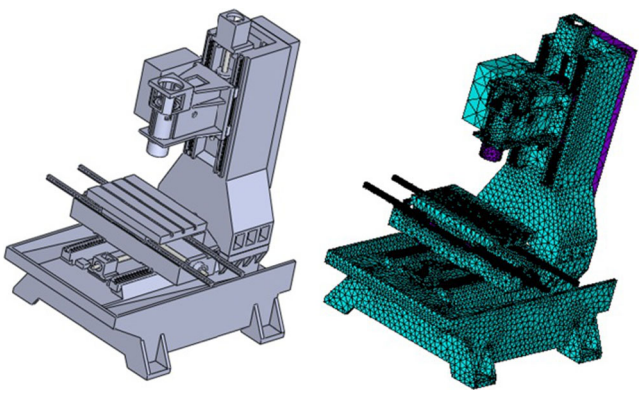

Fig. 13 FEM of the whole machining vertical center

7 Optimization of the whole machine tool

According to the mode shapes of the whole vertical machining center obtained in Section 5, vibrations of the column and headstock are obviously in the frequency range 0~600 Hz. Taking the dynamic flexibility to measure the vibration resistance of the whole vertical machining center [33], we mainly focused on the direct FRFs at the spindle nose in three directions. Observing the frequencies corresponding to the peaks of the FRFs in Fig. 16, the FRFs and the mode shapes can be connected. Mode shapes corresponding to these frequencies mainly represent the bending vibrations and the sway movements of the column and the headstock. Through the analysis above we confirmed that the column and the headstock had a poor vibration resistance in the frequency range 0~600 Hz. Studying their vibrations, they were mainly related to the

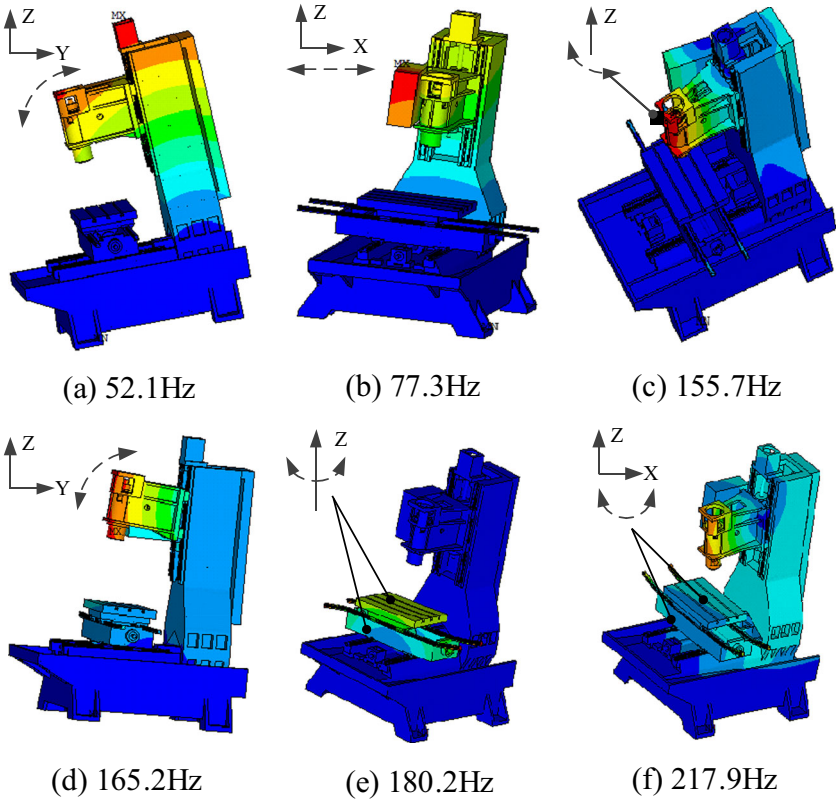

Fig. 14 Fundamental mode shapes of the whole machine tool

joints belonging to them, including the linear guide, the ball screw, the bearing, and the bolt joint.

As researches have shown that the dynamic stiffness of the joints accounts for 60 % of the whole machine tool stiffness [3, 34, 35], it is significant to optimize the characteristics of the whole vertical machining center based on the joints stiffness. The principle and process to implement the optimization are described in the following subsections.

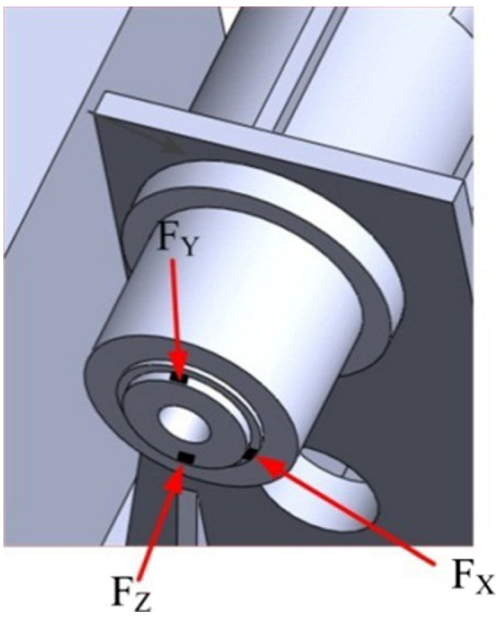

Fig. 15 Directions of the simulated external force

7.1 The optimization principle

Appling the proportional damping into the machine tool structure, the dynamic flexibility between the excitation point A and the response point B can be described as Eq. (27), which is based on the modal theory for vibration characteristics.

$$\frac{X_b}{F_a} = \sum_{r=1}^{\infty} \frac{1}{\left[1-\left(\frac{\omega}{\omega_r}\right)^2 + i2\xi_r\left(\frac{\omega}{\omega_r}\right)\right]}\left(\frac{A_a{}^{(r)}A_b{}^{(r)}}{K_r}\right) \tag{27}$$

$$(f_{ab})_r = \left(\frac{A_a{}^{(r)}A_b{}^{(r)}}{K_r}\right) \tag{28}$$

Where $(f_{ab})_r$ is defined as the rth modal flexibility between the excitation point A and the response point B; $A_a{}^{(r)}$ and $A_b{}^{(r)}$ is the rth relative displacement amplitude of point A and point B respectively; K_r is the rth modal stiffness.

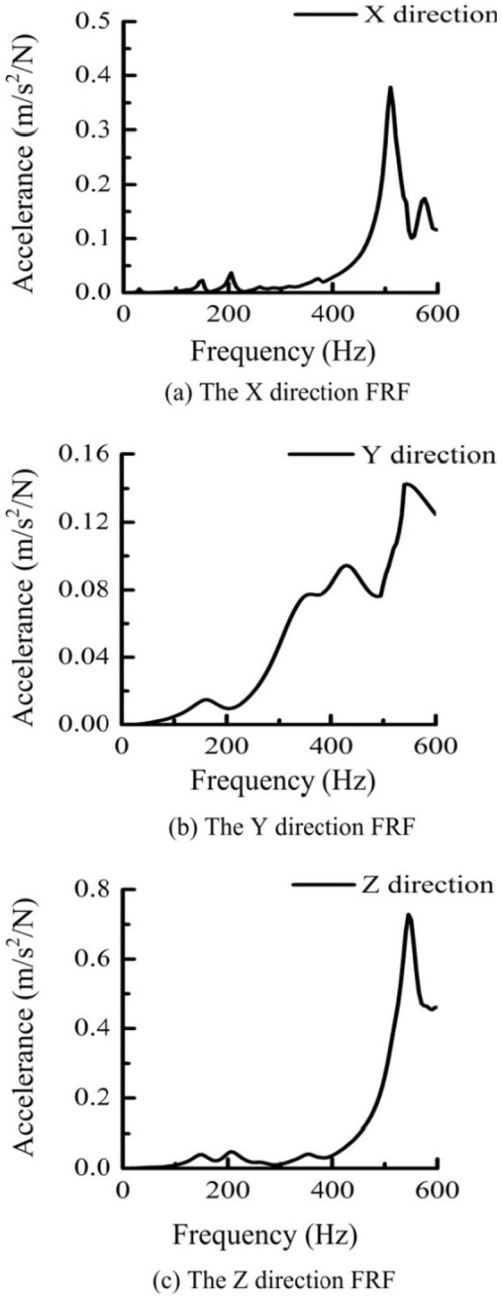

Fig. 16 Simulated FRFs of the spindle nose

If these modes have a small coupling degree, when the machine tool vibrates at the *r*th natural frequency, the dynamic flexibility is mainly determined by the *r*th mode. Thus, Eq. (27) can be described as Eq. (29).

$$\left(\frac{X_b}{F_a}\right)_{\omega\approx\omega_{nr}} = \left(\frac{X_b}{F_a}\right)_r \approx \frac{(f_{ab})_r}{\left[1-\left(\frac{\omega}{\omega_r}\right)^2 + i2\xi_r\left(\frac{\omega}{\omega_r}\right)\right]} \tag{29}$$

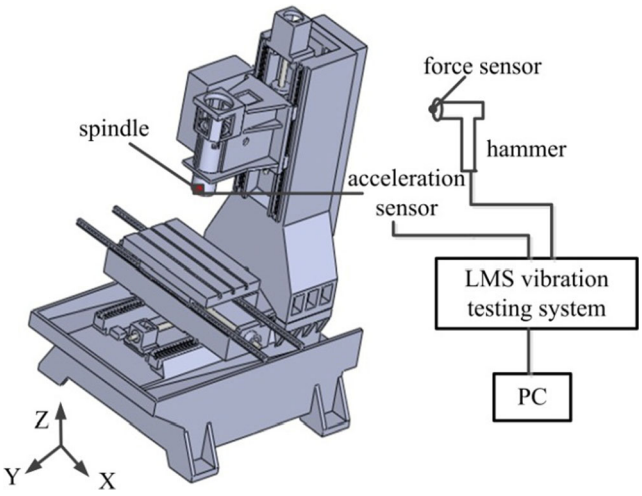

Fig. 17 The experimental devices

When the exciting frequency is close to zero, we can get Eq. (30) and Eq. (31).

$$\left(\frac{X_b}{F_a}\right)_{\omega\to 0} = (f_{ab})_s = \sum_{r=1}^{\infty}(f_{ab})_r \tag{30}$$

$$\frac{\sum_{r=1}^{\infty}(f_{ab})_r}{(f_{ab})_s} = \frac{(f_{ab})_1}{(f_{ab})_s} + \frac{(f_{ab})_2}{(f_{ab})_s} + \cdots\cdots = 1.0 \tag{31}$$

Where $(f_{ab})_s$ is the static flexibility.

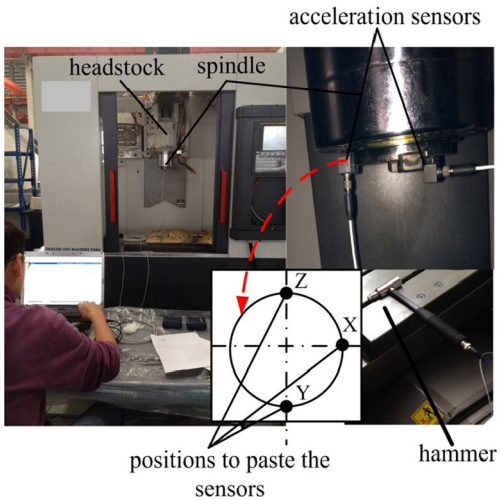

Fig. 18 Vibration experiment of the whole machine tool

Table 7 Parameters related to the vibration experiment

Name	Type	Sensibility	Weight
Impulse hammer	PCB 086D05	0.23 mV/N	0.32 kg
Accelerometer *X*	ICP	99.8 mV/g	4 g
Accelerometer *Y*	ICP	99.3 mV/g	4 g
Accelerometer *Z*	ICP	101.1 mV/g	4 g

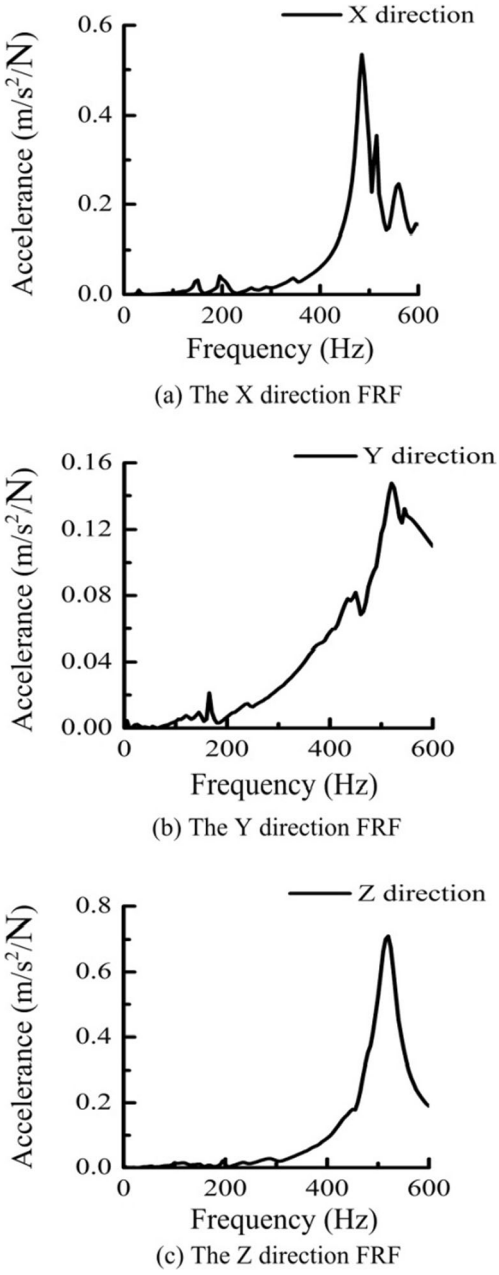

Fig. 19 Experimental FRFs of the spindle nose

Equations (30) and (31) mean that when the exciting frequency is close to zero, the machine tool dynamic flexibility equals the static flexibility as well as the sum of each modal flexibility. $(f_{ab})_r/(f_{ab})_s$ is the ratio between the *r*th modal flexibility and the static flexibility, which reveals the influential degree of the *r*th modal flexibility to the static modal flexibility. If ratios of each mode are roughly equal, it means that the stiffness and the mass of the whole structure are close to the optimal configuration and there are no prominent weak parts.

Based on Eqs. (27) to (31), we can confirm that if each modal flexibility and the static flexibility are as small as possible, a smaller dynamic flexibility can be obtained. Researchers have pointed out that the modes with a higher $(f_{ab})_r/(f_{ab})_s$ are the weak modes, which determine the dynamic characteristics of the structure [32]. Hence, the weak modes of the whole vertical machining center can be determined according to each modal flexibility, the static flexibility, and the ratios between them.

To optimize the characteristics of the machine tool, we aim to decrease the modal flexibility of these weak modes based on the joints stiffness.

7.2 The design variables and objectives

The optimization based on the joint stiffness is to find a group of parameters to describe the contact stiffness of each joint, under which the modal flexibility of the weak modes should be as small as possible.

1. The design variables

   Assuming a system with *N* modules, its elastic energy is the sum of *N* modules' elastic energy. When one module vibrates under the *r*th mode, its elastic energy and the elastic energy of the system can be defined as follows:

$$V_{sr} = \frac{1}{2}\{A^r\}^T[K]_s\{A^r\} \tag{32}$$

$$V_{Ar} = \sum_{s=1}^{n} V_{sr} \tag{33}$$

$$R_s = V_{sr}/V_{Ar} \tag{34}$$

   Where $\{A^r\}$ is the column vector of the displacement amplitudes including all the nodes belonging

Table 8 Frequency results of the simulation and the experiment

	Order									
	1	2	3	4	5	6	7	8	9	10
Experiment (Hz)	56.25	81.25	103.1	118.8	171.9	331.3	378.1	393.8	406.3	425
Simulation (Hz)	52.1	77.30	116.3	130..1	165.2	354.6	395.5	405.5	423.7	442.1
Error (%)	7.97	4.87	12.6	9.5	3.90	7.03	4.6	2.84	4.28	4.02

to the sth module when the system vibrates under the rth mode; $[K]_s$ is the stiffness matrix of the sth module; R_s is the sth module's elastic energy distribution ratio.

Through Eqs. (32) to (34), the elastic energy of the joints and the whole machine tool and the elastic energy distribution ratios under the weak modes can be calculated. Joints with a higher elastic energy distribution ratio are determined to be the weak joints with a lower dynamic stiffness. Then stiffness of these weak joints is taken as the design variables described as Eq. (35).

$$k = \{k_1 \;\; k_2 \;\; \cdots \;\; k_i \;\; \cdots \;\; k_n\}^{\mathrm{T}} \qquad (i = 1, 2, \cdots, n) \quad (35)$$

Where k_i is the stiffness of the ith weak joints.

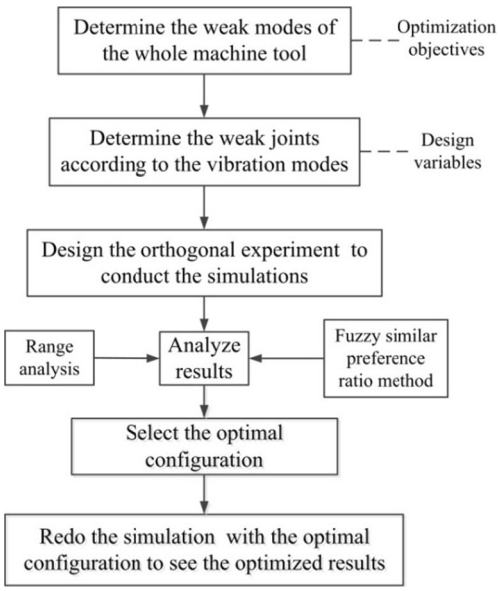

Fig. 20 The flowchart of the optimized method

2. The objectives of the optimization

Taking the minimal modal flexibilities of the weak modes as the objectives, the multiobjective optimization mathematical model are established

$$\begin{gathered} \mathrm{Minimize}(f_{ab})_r = \left(\frac{A_a{}^{(r)} A_b{}^{(r)}}{K_r}\right)(r = 1, 2, \cdots, n) \\ k = \{k_1 \;\; k_2 \cdots k_i \cdots k_n\}^{\mathrm{T}} \quad (i = 1, 2, \cdots, n) \\ s.t. \quad k_{\min} \le k_i \le k_{\max} \end{gathered} \quad (36)$$

Where $(f_{ab})_r$ is the modal flexibility of the rth weak mode.

7.3 The application of the optimized method

The optimization was implemented according to the flowchart as shown in Fig. 20.

1. The weak modes

The direct dynamic flexibilities of the points at the spindle nose in three directions were taken as the criterions to measure the characteristics of the whole vertical machining center. These points were marked as X, Y, and Z in Fig. 18, representing the X, Y, and Z directions respectively.

The simulated static flexibilities in X, Y, and Z directions were 3.191×10^{-8}, 4.387×10^{-8}, and 3.405×10^{-8} N/m. With the relative displacement amplitudes extracted through the modal analysis, the modal flexibilities and the ratios were calculated based on Eqs. (28) and (31). Results are shown in Table 9, which lists the ratios close or above 10 % in the frequency range 0~600 Hz. Six modes were determined to be the weak modes, the minimal modal flexibilities of which were the optimization objectives.

2. The weak joints

As vibrations of the bed, the worktable and the saddle were very faint according to the mode shapes, the

Table 9 Weak modes and the rations

Order	Direction	Modal flexibility (10^{-9} m/N)	Ratio (%)
2	*X*	8.17	25.6
3	*Y*	6.53	14.9
7	*Y*	9.39	21.4
27	*Y*	4.91	11.2
2	*Z*	9.72	28.5
8	*Z*	8.73	25.6
10	*Z*	3.01	8.84

configuration of joints stiffness was focused on the joints belonging to the spindle-column system. These joints included the spindle bearing joint, the linear guide joint in the *Z* direction, the ball screw joint in the *Z* direction and the spindle-column bolt joint. Their joints elastic energy and elastic energy distribution ratios corresponding to the weak modes were calculated from Eqs. (32) to (34). The results are listed in Table 10.

Comparing the data in Table 10, those that have a higher distribution ratio were determined to be the weak joints. Hence, stiffness of the spindle bearing joint, the linear guide joint in the *Z* direction, and the spindle-column bolt joint in the *Z* direction were regarded as the design variables. The spindle-bearing joint stiffness was marked as k_1, the linear guide joint stiffness in the *Z* direction was marked as k_2, and the column-bed bolt joint stiffness was marked as k_3. With the design variables and the optimization objectives, the multiobjective optimization mathematical model were established based on Eq. (36)

3. The orthogonal experiment design

The aim of the optimization is to select an optimal configuration of these joints stiffness to make the modal flexibilities of these week modes as small as possible. However, under different contact conditions, the joints have different stiffness values, it is difficult and a waste of time to study how the stiffness value of each joint influences the characteristics of the whole machine tool. Thus, the orthogonal experiment design method was adopted to improve the calculation efficiency of the optimization [31, 35, 36].

Based on the joint dynamic characteristic parameters identified in the study of this vertical machining center and the select demands used by the machine tool producer to purchase the components including the spindle, the ball screw, and the linear guide, three stiffness values were determined for each design variable. The axial and radial stiffness of the spindle bearing joints were regarded as one factor, and the normal and tangential stiffness of the bolt joints were regarded as another factor. Table 11 lists the factors and levels of the orthogonal experiment.

The orthogonal experiment table $L_9(3^4)$ was adopted to execute nine simulations according to the factors and levels. With the simulated results, modal flexibilities of the weak modes were calculated. Table 12 lists the arrangement of the simulations and the related results.

4. The orthogonal experiment results analysis

Range analysis described as Eq. (37) was used to analyze the influence of the joints stiffness to the modal flexibilities.

$$R_i = \max\left(p_{i1},\cdots,\ p_{ij},\cdots,p_{in}\right) - \min\left(p_{i1},\cdots,p_{ij},\cdots,p_{in}\right) \tag{37}$$

Where p_{ij} (j=1,2, ⋯,n; i=1,2, ⋯,n) is the arithmetic value for the simulated results when the ith factor adopts the jth level. Analyzing the p_{ij} under the same factor, of how this factor affects the experiment results can be studied. Then, one optimal level for this factor

Table 10 Elastic energy distribution ratio

Joints	Distribution ratio (%)					
	2	3	7	8	10	27
Bearing	1.51	2.06	1.01	3.42	4.98	37.2
Linear guide	8.19	9.98	40.8	38.5	45.7	8.63
Ball screw	3.88	0.42	4.52	1.01	1.42	3.34
Bolt joint	30.9	46.7	8.03	9.97	12.1	4.83

Table 11 Orthogonal factor level table

Level	Stiffness (N/m)				
	k_1		k_2	k_3	
	axial	radial		normal	tangential
1	5.3×10^{7}	3.45×10^{8}	5.83×10^{8}	4.63×10^{10}	6.9×10^{9}
2	1.10×10^{8}	5.52×10^{8}	7.67×10^{8}	6.02×10^{10}	8.28×10^{9}
3	1.58×10^{8}	7.11×10^{8}	9.33×10^{9}	7.04×10^{10}	9.94×10^{9}

Table 12 Results of the orthogonal experiment

Order	Factor			Modal flexibility (10^{-9} m/N)						
	k_1	k_2	k_3	$(f_{ab})_2$		$(f_{ab})_3$	$(f_{ab})_7$	$(f_{ab})_8$	$(f_{ab})_{10}$	$(f_{ab})_{27}$
1	1	1	1	8.17	9.72	6.53	9.39	8.73	3.01	4.91
2	1	2	2	8.07	9.69	6.51	9.15	8.45	3.05	4.61
3	1	3	3	7.69	9.68	6.49	9.11	8.27	3.09	4.35
4	2	1	2	8.05	9.65	6.61	9.49	8.01	2.63	5.29
5	2	2	3	7.94	9.63	6.52	9.32	7.73	2.62	5.21
6	2	3	1	7.91	9.59	6.49	9.23	7.56	2.59	5.14
7	3	1	3	7.35	9.32	6.46	9.09	7.87	2.53	4.85
8	3	2	1	7.59	9.47	6.52	9.15	7.55	2.54	4.77
9	3	3	2	7.47	9.34	6.51	9.17	7.39	2.57	4.73

can be obtained. Based on the optimal level for each factor, the optimal configuration of these factors are determined. R_i is the result of the range analysis, which represents the influential degree of the ith factor to the simulated results. The higher the R_i, the more significantly the ith factor influences the simulated results. Comparing these results of the range analysis, the affecting orders of these factors can be obtained.

The optimization studied on the vertical machining center in this paper belongs to a multiobjective optimization problem. Thus, in order to use the range analysis to analyze the results, the fuzzy similar preference ratio method was adopted to change the multiobjective problem into a single objective problem [37, 38]. Application of the fuzzy similar preference ratio method is as follows (Fig. 21):

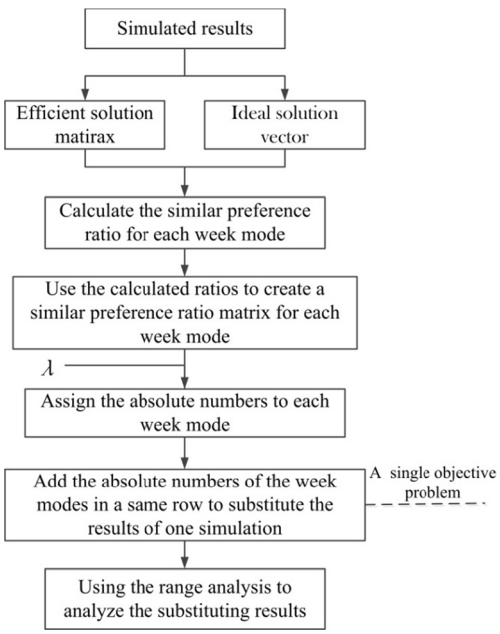

Fig. 21 Flowchart of the fuzzy similar preference ratio method

(1) Take the nine sets of modal flexibilities in the orthogonal Table 12 to compose the efficient solution matrix $\boldsymbol{F}^*$ for the multiobjective problem.

$$F^* = \begin{bmatrix} f_{11} & \cdots & f_{1r} & \cdots & f_{17} \\ \vdots & \vdots & \vdots & \vdots & \vdots \\ f_{k1} & \cdots & f_{kr} & \cdots & f_{k7} \\ \vdots & \vdots & \vdots & \vdots & \vdots \\ f_{91} & \cdots & f_{9r} & \cdots & f_{97} \end{bmatrix} \tag{38}$$

Where f_{kr} (k=1,2, ⋯,9; r=1,2, ⋯,7) is the modal flexibility of rth weak mode under the kth simulation.

(2) Take the minimal modal flexibility of each weak mode in Table 12 to compose the ideal solution $\boldsymbol{F}$ for the multiobjective problem.

$$F = [\,(f_1)_{\min} \quad \cdots \quad (f_r)_{\min} \quad \cdots \quad (f_7)_{\min}\,] \tag{39}$$

Where $(f_r)_{\min}$ (r=1,2, ⋯,7) is the minimal modal flexibility of the rth weak mode.

(3) Calculate the fuzzy similar preference ratio by Eq. (40) and measure the similarity between each efficient solution and the ideal solution. The efficient

Table 13 Results of the similarity priority ratio method

Experiment order	Factor			Absolute priority number							Sum
	k_1	k_2	k_3	$(f_{ab})_2$		$(f_{ab})_3$	$(f_{ab})_7$	$(f_{ab})_8$	$(f_{ab})_{10}$	$(f_{ab})_{27}$	
1	1	1	1	9	9	8	8	9	7	6	56
2	1	2	2	8	8	5	4	8	8	2	43
3	1	3	3	4	7	3	2	7	9	1	33
4	2	1	2	7	6	9	9	6	4	9	50
5	2	2	3	6	5	7	7	4	5	8	42
6	2	3	1	5	4	4	5	2	6	7	33
7	3	1	3	1	1	1	1	5	1	5	16
8	3	2	1	3	3	6	3	3	2	4	24
9	3	3	2	2	2	2	6	1	3	3	19

solution with a higher fuzzy similar preference ratio means it is closer to the optimal solution.

$$r_{rst} = \frac{\left|(f_r)_{\min} - f_{tr}\right|}{\left|(f_r)_{\min} - f_{sr}\right| + \left|(f_r)_{\min} - f_{tr}\right|} \tag{40}$$

Where r_{rst} is the similar preference ratio, f_{sr} and f_{tr} (s, t=1,2, ⋯,9) are the sth and tth simulated modal flexibility of the rth weak mode respectively. Assume that r_{rss}=r_{rtt}=1. When 0.5<r_{rst}≤1, f_{sr} is prior to f_{tr}. When 0<r_{rst}<0.5, f_{tr} is prior to f_{sr}. But if r_{rst}= 0.5, the priority cannot be determined.

With the calculated similar preference ratios, the similar preference ratio matrix $\boldsymbol{M_r}$ of the rth weak mode can be established.

$$M_r = \begin{bmatrix} r_{r11} & r_{r12} & \cdots & r_{r19} \\ r_{r21} & r_{r22} & \cdots & r_{r29} \\ \vdots & \vdots & \cdots & \vdots \\ r_{r91} & r_{r92} & \cdots & r_{r99} \end{bmatrix} \tag{41}$$

Select a λ, which is 0.5 in this paper. If r_{rst}≥λ, replace the r_{rst} with 1. If r_{rst}≤λ, replace the r_{rst} with 0. In the matrix $\boldsymbol{M_r}$, a row whose similar preference ratios are all replaced with 1 is marked with an absolute preference number. This number is used to substitute the modal flexibility of the rth weak mode in the same row in Table 12. Then, delete the row and the column with a same sequence number, and chose another row whose similar preference ratios are all replaced with 1. Repeat this process until all the rows have an absolute preference number. Numbers are from 1 to 9 in this paper and are assigned based on the order of the row replaced all by 1.

As all the absolute preference numbers of each weak mode were calculated, add up these numbers in a same row in the Table 13 to represent the results of one simulation to do the range analysis.

Based on the range analysis and fuzzy similar preference ratio method developed above, results are listed in Tables 13 and 14.

From Table 14, we can determine that stiffness of the spindle ball screw joint affects the characteristics of the whole machine tool more heavily and stiffness

Table 14 Results of the range analysis

Experiment order	Factor			Sum
	k_1	k_2	k_3	
1	1	1	1	56
2	1	2	2	43
3	1	3	3	33
4	2	1	2	50
5	2	2	3	42
6	2	3	1	33
7	3	1	3	16
8	3	2	1	24
9	3	3	2	19
P_{11}, P_{21}, P_{31}	44	40.1	37.7	
P_{12}, P_{22}, P_{32}	41.7	36.3	37.3	
P_{13}, P_{23}, P_{33}	19.7	28.3	30.3	
R_1, R_2, R_3	24.3	11.8	7.4	
Influence sequence	k_1>k_2>k_3			
Optimal factor	3	3	3	
Optimal configuration	$(k_1)_3(k_2)_3(k_3)_3$			

Table 15 Results of the optimization

Order	Modal flexibility (10^{-9} m/N)		Frequency (Hz)		Rate of change (%)	
	Before optimization	After optimization	Before optimization	After optimization	Modal flexibility	Frequency
$(f_{ab})_2$	8.17	7.31	52.1	54.6	10.5	4.58
	9.72	9.26	52.1	54.6	4.73	4.58
$(f_{ab})_3$	6.53	6.38	77.3	79.5	2.85	2.59
$(f_{ab})_7$	9.39	8.99	155.7	159.2	2.25	2.25
$(f_{ab})_8$	8.73	7.32	165.2	168.5	16.2	2.00
$(f_{ab})_{10}$	3.01	2.49	207.3	213.9	17.3	3.18
$(f_{ab})_{27}$	4.91	4.41	501.5	508.8	10.2	1.46

of the column-bed bolt joint affects the least. The optimal configuration of the joints stiffness is $(k_1)_3(k_2)_3(k_3)_3$.

5. Simulation with the optimal configuration

Appling the optimal configuration of the joint stiffness into the FEM to have a modal analysis, modal flexibilities of the weak modes were calculated. Results are shown in Table 15, in which the natural frequencies before and after the optimization are also included.

Observing Table 15, the 2nd mode in the *X* direction, the 8th and 10th modes in the *Z* direction and the 27th mode in the *Y* direction have an obvious decrease in the modal flexibility, which are down to 10.5, 16.2, 17.3, and 10.2 % respectively. The 2nd mode in the *Z* direction and the 3rd and 7th modes in the *Y* direction have a decrease in the modal flexibility about 4.73, 2.85, and 2.25 %, respectively. The natural frequencies corresponding to the weak modes are also improved. The 2nd natural frequency obtains the maximum increase by 4.58 %.

The direct FRFs at the spindle nose in three directions after the optimization are depicted in Fig. 22. Comparing Fig. 22 with Figs. 16 and 19, frequencies corresponding to the peaks have a little change and the amplitudes are decreased as the joints stiffness increased.

The decreased modal flexibilities and dynamic responses validate the feasibility of the optimization.

8 Conclusions

The dynamical characteristics optimization of a vertical machining center based on the configuration of joint stiffness is presented in this paper. As methods to identify the joint parameters were developed, the studied FEM of the whole vertical machining center was created considering the dynamic characteristics of the joints, the accuracy of which were verified by the comparison between the vibration tested and simulated results. Using the dynamic flexibility to measure the vibration resistance of the whole vertical machining center, the weak modes and joints were determined by applying the modal flexibility and elastic energy distribution theory. Orthogonal experiment was applied to instruct the optimization to find an optimal configuration of stiffness to decrease the modal flexibility of the weak modes. The range analysis and fuzzy similar preference ratio method were used to analyze the results of the optimization. The determined optimal configuration of joint stiffness was applied in the FEM to redo the simulation. The decreased modal flexibilities and dynamic responses validated the feasibility of this method. Major conclusions are drawn as follows:

1. FEM of the whole vertical machining center based on the characteristics of the joints was verified to be accurate by the experiment. Thus, this model could be used to simulate and predict the characteristics of the whole vertical machining center accurately.

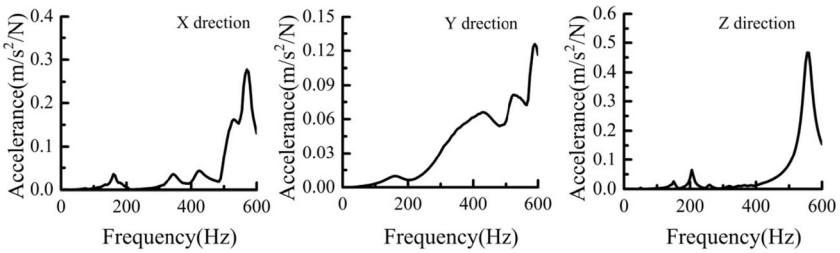

Fig. 22 FRFs after the optimization in three directions

2. With the modal flexibility and the elastic energy distribution theory, weak modes and weak joints of the vertical machining center has been determined efficiently.
3. Optimization efficiency was improved by combining the orthogonal experiment method, the range analysis and the fuzzy similar preference ratio method to solve the multiobjective problem.
4. The studied joints stiffness can provide a basic theory support for the machine tool producer to purchase the ball screw, the linear guide, and the spindle.

Acknowledgments This research is sponsored by National Science and Technology Major Project of China and Science and Technology Support Project of Sichuan Province. (NO.2013ZX04005-012 and NO.2012GC0008).

References

1. Liang YC, Chen WQ, Bai QS, Sun YZ, Chen GD, Zhang Q, Sun Y (2013) Design and dynamic optimization of an ultraprecision diamond flycutting machine tool for large KDP crystal machining. Int J Adv Manuf Technol 69:237–244
2. Lee SW, Mayor R, Ni J (2005) Dynamic analysis of a mesoscale machine tool. J Manuf Sci Eng 128(1):194–203
3. Zhang GP, Huang YM, Shi WH, Fu WP (2003) Predicting dynamic behaviors of a whole machine tool structure based on computer-aided engineering. Int J Mach Tools Manuf 43:699–706
4. Fu WP, Huang YM, Zhang GP (1993) Experimental investigation on damping behavior of normal joint surface at unit area. Model Meas Control B 51:13–20
5. Lee U (2001) Dynamic characterization of the joints in a beam structure by using spectral element method. Shock Vib 8(6):357–366
6. Lin Y, Chen W (2002) A method of identifying interface characteristic for machine tools design. J Sound Vib 255:481–487
7. Hwang HY (1998) Identification techniques of structure connection parameters using frequency response function. J Sound Vib 212(3): 469–479
8. Yang TC, Fan SH, Lin CS (2003) Joint stiffness identification using FRF measurements. Comput Struct 81:2549–2556
9. Li DS, Zhang YD, Wang P (2010) Dynamic model of machine joints based on structural damping. J Vib Shock 29:204–208
10. Hung JP (2009) Load effect on the vibration characteristics of a stage with rolling guides. J Mech Sci Technol 23:92–102
11. Wang JH, Chuang SC (2004) Reducing errors in the identification of structural joint parameters using error functions. J Sound Vib 273(1–2):295–316
12. Schmitz TL, Donalson RR (2000) Predicting high-speed machining dynamics by substructure analysis. CIRP Ann Manuf Technol 49(31):303–308
13. Hung JP, Lai YL, Luo TZ (2013) Analysis of the machining stability of a milling machine considering the effect of machine frame structure and spindle bearings: experimental and finite element approaches. Int J Adv Manuf Technol 68:2393–2405
14. Kolar P, Sulitka M, Janota M (2011) Simulation of dynamic properties of a spindle and toolsystem coupled with a machine tool frame. Int J Adv Manuf Technol 54:11–20
15. Ahmadian H, Jalali H (2007) Identification of bolted lap joints parameters in assembled structures. Mech Syst Signal Process 21: 1041–1050
16. Mao KM, Li B, Wu J, Shao X (2010) Stiffness influential factors-based dynamic modeling and its parameter identification method of fixed joints in machine tools. Int J Mach Tools Manuf 50:156–164
17. Lin QY, Hung JP, Lo TL (2010) Effect of preload of linear guides on dynamic characteristics of a vertical column-spindle system. Int J Mach Tools Manuf 50:741–746
18. Wu JSS, Chang JC, Hung JP (2007) The effect of contact interface on dynamic characteristics of composite structures. Math Comput Simul 74:454–467
19. Yoshihara M (1979) Computer-aided design improvement of machine tool states incorporating joint dynamics data. Ann CIRP 28: 241–246
20. Park SS, Chae J (2008) Joint identification of modular tools using a novel receptance coupling method. Int J Adv Manuf Technol 35: 1251–1262
21. Sun MN, Yin GF, Hu T (2013) Orthogonal optimization method of dynamic stiffness of machine tool joints based on modal flexibility. J Sichuan Univ (Eng Sci Ed) 45:90–96
22. Sun MN, Yin GF, Hu T, Hu XB (2013) Method of dynamic stiffness participation factors identification of machine tool joints based on the generalized dynamic information mode. J Mech Eng 49:61–69
23. Mi L, Yin GF, Sun MN (2012) Effects of preloads on joints on dynamic stiffness of a whole machine tool structure. J Mech Sci Technol 26:495–508
24. Jiang SY, Zhu SL (2010) Dynamic characteristic parameters of linear guideway joint with ball screw. J Mech Eng 4:92–99
25. Patwari AU, Faris WF, Nurul Amin AKM, Loh SK (2009) Dynamic modal analysis of vertical machining centre components. Adv Acoust Vib
26. Marghitu DB (2001) Mechanical engineer's handbook. Academic, San Diego
27. Carvill J (1993) Mechanical engineer's data handbook. Butterworth-Heinemann, Burlington
28. Liao BY, Zhou XM, Yin ZH (2004) Modern mechanical dynamics and its application: modeling, analysis, simulation, modification, control, optimization. Beijing
29. Zhang XL (2002) The dynamic characteristics of machine joint surface and its application. Beijing
30. Huang JP, Lai YL, Lin CY, Lo TL (2011) Modeling the machining stability of a vertical milling machine under the influence of the preloaded linear guide. Int J Mach Tools Manuf 51:731–739
31. PMI Technologies Company. Ballscrew/Linear guideway/Mono stage general catalog: ball screw. http://www.pmi-amt.com/cn/support/download.html
32. Gao XS, Zhang YD, Zhang HW, Wu Q (2012) Effects of machine tool configuration on its dynamics based on orthogonal experiment method. Chin J Aeronaut 25:285–291
33. Yang X, Tang HL, Liao BY (1983) Machine tool dynamics. Beijing
34. Yang Y, Wang LP (2005) Finite Element Model Updating Method and Its Application. Conference & Exposition on Structural Dynamics, Orlando, Florida, USA
35. Mohan LV, Shunmugam MS (2006) An orthogonal array based optimization algorithm for computer-aided measurement of worm surface. Int J Adv Manuf Technol 30:434–443
36. Xu F, Zhang LB, Jiang JD, Z X (2008) Optimization method of agricultural machinery handle based on FEA and orthogonal experimental design. Chin J Mech Eng 44:245–249
37. Arghavani J, Derenne M, Marchand L (2001) Sealing performance of gasketed bolted flanged joints: a fuzzy decision support system approach. Int J Adv Manuf Technol 17:2–10
38. He XG (1994) Fuzzy Database System. Beijing